Wu and Banerjee *AAPPS Bulletin* (2022) 32:19
https://doi.org/10.1007/s43673-022-00048-1

AAPPS Bulletin

REVIEW ARTICLE Open Access

The production of actinides in neutron star mergers

Meng-Ru Wu[1,2*] and Projjwal Banerjee[3*]

Abstract

Although the multimessenger detection of the neutron star merger event GW170817 confirmed that mergers are promising sites producing the majority of nature's heavy elements via the rapid neutron-capture process (*r*-process), a number of issues related to the production of translead nuclei—the actinides—remain to be answered. In this short review paper, we summarize the general requirements for actinide production in *r*-process and the impact of nuclear physics inputs. We also discuss recent efforts addressing the actinide production in neutron star mergers from different perspectives, including signatures that may be probed by future kilonova and γ-ray observations, the abundance scattering in metal-poor stars, and constraints put by the presence of short-lived radioactive actinides in the Solar system.

Keywords: *r*-process, Neutron star merger

1 Introduction

The detection of the kilonova accompanying the gravitational wave emissions from the binary neutron star merger (BNSM) event GW170817 [1, 2] provided a first direct evidence that the rapid neutron-capture process (*r*-process) takes place in BNSMs (see refs. [3–7] for recent reviews and references therein). This discovery also offers new insights on a number of key issues including, e.g., the nature of dense matter and the expansion rate of the universe [8–22]. However, the comparison of the observed spectroscopic and photometric data to theory models only confirmed the existence of heavy elements with high atomic opacity [23–27], likely lanthanides, as well as the potential signature of lighter *r*-process elements such as strontium [28] (see also [29–31]). Whether or not even heavier nuclear isotopes—the actinides—can be produced in BNSM events remain unclear (cf. [32]).

On the other hand, quite a number of metal-poor stars in our galaxy enriched by the *r*-process also contain thorium whose relative abundance to the lanthanides are similar to those in our Solar system (see, e.g., Refs. [33, 34] for reviews). This indicates that the major *r*-process(es) producing astrophysical sites should also produce certain amount of actinides. Attempts to use the actinide abundances in metal-poor stars to date their ages and therefore connect to the age of the Universe through the so-called nuclear cosmochronometry have been made in [35–40]. Moreover, short-lived radioactive actinide isotopes whose life times are on the order of few million years (Myrs), have been shown to be present currently in the Earth's deep-sea crusts. Additionally, isotopic anomalies in meteorites clearly show that such radioactive isotopes were present at the time of formation of the Solar system. These detection have been used as direct evidence of the production of actinides by BNSMs or to constrain the *r*-process conditions in potential production sites [41–46].

In this article, we review recent efforts that addressed the issue of actinide production by *r*-process in BNSMs. In Section 2, we discuss the astrophysical conditions allowing for actinide production in BNSMs and the impact of uncertain nuclear physics inputs. In Section 3, we highlight recently proposed features associated with actinide production that may be detected by future kilonova observations or the next-generation γ-ray telescopes. Section 4

*Correspondence: mwu@gate.sinica.edu.tw; projjwal.banerjee@gmail.com
[1]Institute of Physics, Academia Sinica, Taipei 11529, Taiwan
Full list of author information is available at the end of the article

focuses on the observation of actinide abundances in metal-poor stars and their implications. Section 5 discusses the implications of measurements of the short-lived radioactive isotopes on actinide production in BNSMs. We conclude this review in Section 6.

2 Theory requirements and nuclear physics inputs

Earlier r-process nucleosynthesis studies that adopted either the parametrized BNSM ejecta properties or the outflow trajectories extracted from numerical simulations modeling the post-merger evolution of BNSMs, revealed that a significant amount of actinides with mass fraction $X_{\rm act} \gtrsim 10^{-3}$ is only produced in ejecta with $Y_e \lesssim 0.2$ [47–60]. This can be qualitatively understood from relating the averaged nuclear mass number at the end of the r-process ($\langle A\rangle_f$) to the averaged initial seed nuclear mass number ($\langle A\rangle_s$) and the abundance ratio of free neutrons to seed nuclei ($R_{n/s}$) before the onset of r-process by

$$\langle A\rangle_f = \langle A\rangle_s + R_{n/s}. \tag{1}$$

Assuming that right before the onset of r-process (usually around $T \simeq 3-5$ GK), the nuclear composition is dominated by free neutrons, with the presence of a small amount of seed nuclei formed via charged-particle reactions (or the α-process) [61], the neutron-to-seed ratio $R_{n/s}$ can be related to the electron fraction Y_e of the ejecta by

$$R_{n/s} = \frac{\langle Z\rangle_s - Y_e\langle A\rangle_s}{Y_e}, \tag{2}$$

where $\langle Z\rangle_s$ is the averaged initial seed nuclear charge number. To produce a significant amount of actinides, the r-process nucleosynthesis needs to proceed beyond the third peak at $A \simeq 195$, which corresponds to $\langle A\rangle_f \gtrsim 150$ [51]. Using this condition together with Eqs. (1) and (2), and considering typical values of $\langle Z\rangle_s \simeq 30$ and $\langle A\rangle_s \simeq 80$, one gets $Y_e \lesssim 0.2$ as the rough threshold value for actinide production in BNSM ejecta. Figure 1 shows the actinide mass fractions $X_{\rm act}$ as a function of Y_e computed after a time evolution of one day (24 hrs) for a typical parametrized BNSM ejecta trajectory, with an initial entropy per nucleon $s = 10\ k_B$ and a dynamical timescale $\tau = 10$ ms used in [62] (see [51] for the form of parametrization), but supplied with different nuclear physics inputs. It clearly shows that although different nuclear physics inputs give rise to quantitatively different amount of actinides for a given value of Y_e, the actinide mass fractions all drop to less than 10^{-4} at values of $Y_e \gtrsim 0.2$. Current BNSM and post-merger simulations suggest that actinides with $X_{\rm act} \gtrsim 10^{-3}$ can be produced in outflows containing a non-negligible component of $Y_e \lesssim 0.2$, ejected dynamically during the merging phase (due to tidal disruption or BNS collision) as well as from post-merger accretion disk outflows with a central black hole or short-lived hyper-massive neutron star that collapses to a black hole within $\sim$ tens of ms [47–50, 52, 53, 57–60].

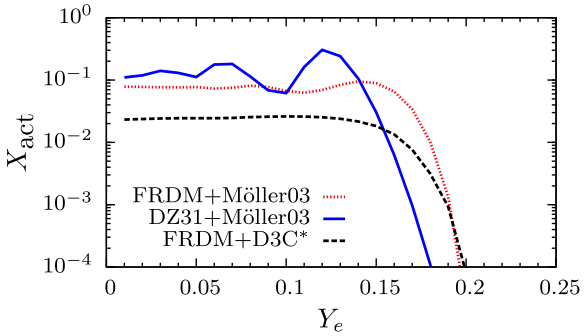

Fig. 1 The actinide mass fraction $X_{\rm act}$ as a function of Y_e for a trajectory with an initial entropy per nucleon $s = 10\ k_B$ and a dynamical timescale $\tau = 10$ ms. The red dotted, blue solid, and black dashed lines are obtained with different combinations of theoretical nuclear mass models (FRDM or DZ31) and ("+") β-decay rates (Möller03 or D3C*)

Let us now discuss the impact of nuclear physics inputs on actinide production. As studied in Refs. [54, 56, 62–72], the theoretical nuclear physics inputs such as the nuclear mass predictions, the β-decay half-lives of translead nuclei, and their fission properties can all greatly impact the production of actinides. This is clearly demonstrated by Fig. 1, where variation of up to a factor of ~ 10 in $X_{\rm act}$ is found for the same Y_e when using different nuclear physics inputs based on two nuclear mass models—the Finite Range Droplet Model (FRDM) [73] and the Duflo-Zuker mass formula with 31 parameters (DZ31) [74]—used in [52, 66], combined with two different β-decay rates from [75] (labeled by Möller03) and [76] (labeled by D3C*).

The effect of nuclear masses comes in mainly through the change of the r-process path, which can be defined by a set of nuclei, each of which is the most abundant one in an isotopic chain. For r-process that operates at temperature that is high enough ($T \gtrsim 0.7$ GK) so that the balance between the neutron captures and photo-dissociations, i.e, the $(n,\gamma) \leftrightarrow (\gamma,n)$ equilibrium, can be maintained, the r-process path locates at nuclei that have two-neutron separation energy S_{2n} just above [77]

$$S^0_{2n} = \frac{T_9}{2.52}\left(34.075 - \log n_n + \frac{3}{2}\log T_9\right), \tag{3}$$

where T_9 is the temperature in GK and n_n is the free neutron number density. Thus, changes in nuclear mass prediction affect how far away from stability the r-process path locates on the nuclear chart. Then, due to the typical condition close to the steady β flow during the r-process, the abundances of neighboring isotopic chains satisfy [78]

$$Y(Z)\langle\lambda_\beta(Z)\rangle = Y(Z+1)\langle\lambda_\beta(Z+1)\rangle, \tag{4}$$

where $Y(Z) = \sum_A Y(Z,A)$ is the total nuclear abundance of an isotopic chain with proton number Z, and $\langle\lambda_\beta(Z)\rangle = \sum_A \lambda_\beta(Z,A)Y(Z,A)/Y(Z)$ is the averaged β-decay rate of the same chain. Because $\langle\lambda_\beta(Z)\rangle$ may be well approximated by λ_β of the nuclei on the r-process path, Eq. (4) implies the following: for two different r-process calculations that have the same β-decay inputs, the case where the r-process path locates further away from the stability in a certain region will have lower nuclear abundances in that region when compared to the other case.

In Fig. 2, we show in panel (a) the comparison of the abundance $Y(A)$ at the time when $R_{n/s} = 1$ for $Y_e = 0.07$ for cases with FRDM+Möller03 and DZ31+Möller03, in panel (b) the corresponding r-process paths, and in panel (c) the $S_{2n}(N)$ for $Z = 78$ around $A = 230$. Panel (b) clearly shows that the FRDM mass model results in a path further away from the stability than the DZ31 case. The corresponding $Y(A)$ around the same mass number range are also a factor of a few smaller than the DZ31 case as shown in panel (a). This difference originates from different evolution of S_{2n} in mass models shown in panel (c). The DZ31 model predicts a faster decline of S_{2n} than FRDM in the actinide region, which results in an r-process path closer to stability and higher actinide abundances as discussed above.

For β-decays, their impact on the actinide abundances comes in directly through Eq. (4). Models that predict relatively faster decay rates in region of actinides compared to other parts of the nuclear chart lead to generally smaller amount of actinide production [54]. Comparing the two example β-decay models, Möller03 and D3C*, Fig. 3a shows that D3C* predicts shorter half-lives than Möller03 by $\sim$ a factor of $\mathcal{O}(10)$ for $A \gtrsim 200$. This then results in smaller actinide abundances during the r-process as shown in panel (b) for cases with $Y_e = 0.07$, and is the primary reason for the generally lower $X_{\rm act}$ shown in Fig. 1 for D3C*.

The properties of nuclear fission can also substantially affect the actinide abundances in r-process with low enough initial $Y_e \lesssim 0.1$ obtained in, e.g., the tidally disrupted material in BNSMs or NS—black hole mergers [68, 70, 72]. These impacts can be generally classified as *direct* and *indirect* ones [70]. The theory dependent prediction of fission barrier and fission path for neutron-rich nuclei of $A \gtrsim 250$ directly determines the relevant fission rates.

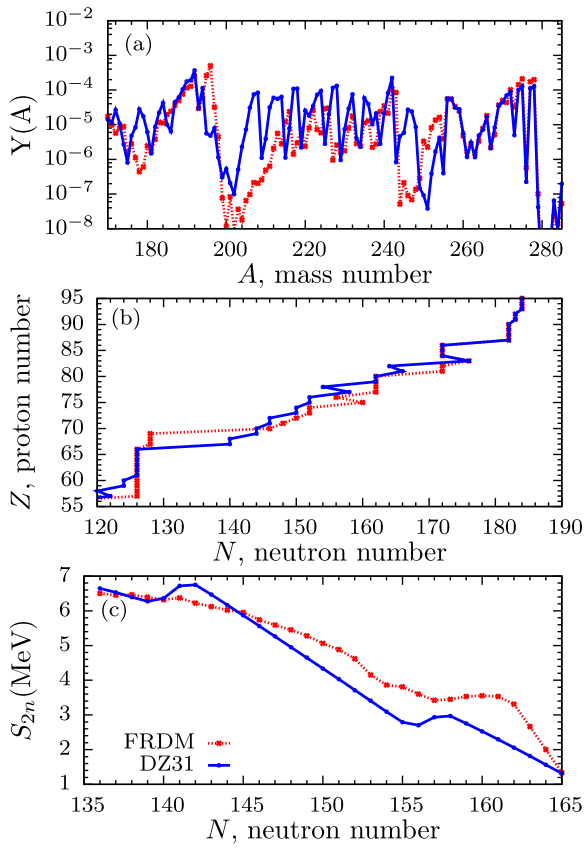

Fig. 2 Comparison of the abundance $Y(A)$ (**a**), r-process path (**b**), and the two-neutron separation energy $S_{2n}(N)$ for $Z = 78$ (**c**) from calculations with $Y_e = 0.07$, for trajectory with an initial entropy per nucleon $s = 10\ k_B$ and a dynamical timescale $\tau = 10$ ms. The red dotted and blue solid lines are obtained with the FRDM and the DZ31 mass model, respectively. For both cases, $S^0_{2n} \simeq 3$ MeV

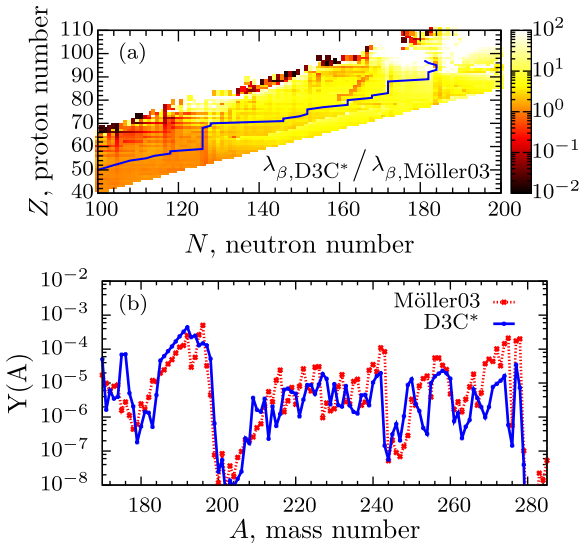

Fig. 3 a The ratio of β-decay rates from D3C* [76] and Möller03 [75] models. The blue line shows the r-process path obtained from a calculation with $Y_e = 0.07$, an initial entropy per nucleon $s = 10\ k_B$, and a dynamical timescale $\tau = 10$ ms, using the FRDM mass model and the D3C* β-decay rates at the time when $R_{n/s} = 1$. **b** The comparison of abundances for $A \geq 170$ using the same trajectory. Both lines are with the FRDM mass model, while the D3C* (Möller03) β-decay rates are used for the blue (red) line

After the r-process freeze-out, when all decay channels (including fission) start to compete, higher fission barriers (or lower fission rates) along relevant isobaric chains can lead to a higher amount of actinides surviving against fission [68, 70]. Consequently, this can result in a larger amount of actinides with $A \gtrsim 250$ at times relevant for kilonova observation (see next section for the particular importance of ^{254}Cf).

The fission rate predictions, together with other rates, also determine the free neutron abundance post the r-process freeze-out via a quasi-equilibrium condition found in [70]. This can lead to more than one order of magnitude difference in free neutron abundance. Cases with larger post freeze-out free neutron abundances undergo more neutron-induced fission, which then results in less $A \gtrsim 250$ actinides that survive against fission. Moreover, a larger amount of free neutrons can also transport non-fissioning actinides of $220 \lesssim A \lesssim 230$ to higher masses, which then affects the α-decay heating relevant for kilonovae (see also next section).

The above discussions outline the major impact of uncertain nuclear physics inputs on the actinide production in merger ejecta. Further development in nuclear theory modeling, e.g., [79–84], will continue to improve our understanding in this aspect. In the next section, we will discuss how they can possibly leave imprints on kilonova emission of BNSMs.

3 Potential electromagnetic observables

The unstable nuclei produced by r-process in the BNSM ejecta within the timescale of $\sim \mathcal{O}(1)$ s gradually decay back to the stability while the ejecta expands. The released nuclear energy from all possible decay channels, including β-decays, α-decays, and different kinds of fission (neutron-induced, β-induced, spontaneous, γ-induced, etc.) directly powers the electromagnetic emission—kilonova—at epochs when thermalized photons can escape, which happens roughly after $\mathcal{O}(1)$ days post the merger [3, 85–88]. Modeling the kilonova lightcurve and spectral evolution plays a decisive role in extracting the underlying properties of the expanding ejecta from observation [23, 27, 89–97].

For this purpose, it was realized in recent years that the exact amount of actinide present in BNSM ejecta can critically affect the amount of the radioactive heating relevant for kilonovae [62, 68–71, 89, 98–100]. For instance, Refs. [89] and [98] first found that the radioactive heating rate (after taking into account the effect of particle thermalization) differ by a factor of 2–6 during $\sim 1-10$ days when adopting different nuclear mass models shown in Fig. 1, for very neutron-rich ejecta with $Y_e \lesssim 0.1$. The origin of this difference can be related to the produced amount of nuclei that α decay at relevant times. Later, Ref. [62] further identified that specifically the α-decay nuclei ^{222}Rn, ^{224}Ra, ^{223}Ra and ^{225}Ac with half-lives $t_{1/2}$ of 3.8, 3.6, 11.43, and 10.0 days[1], as well as the spontaneous fissioning nuclei ^{254}Cf ($t_{1/2} = 60.5$ days), can potentially leave interesting imprints on the bolometric kilonova lightcurve at $t \gtrsim 10$ days (see Fig. 4). Around the same time, Ref. [69] studied independently the impact of ^{254}Cf on certain bands of the lightcurves and reached similar conclusion. These findings suggest that a precise measurement of future kilonova late-time lightcurves from BNSM events can possibly be used to infer the presence of α-decay actinides to the abundance level of $\sim 10^{-5}$ and ^{254}Cf to $\sim 10^{-6}$. More recently, Ref. [71, 100] suggested that the uncertainty from nuclear physics inputs on the kilonova heating rate can be as large as one order of magnitude even at the peak time, based on results that explored outflow conditions with single Y_e values.

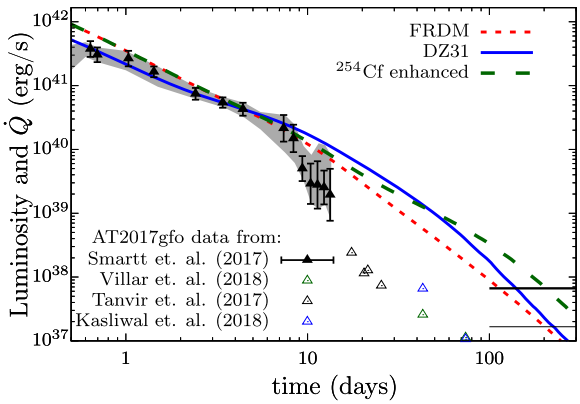

Fig. 4 Impact of the existence of actinides on the bolometric lightcurve of kilonovae. The dotted red, solid blue, and dashed green lines (labeled by FRDM, DZ31, and ^{254}Cf enhanced) represent cases where the lightcurves are dominated by the energy release from β-decays, α-decay actinides, and spontaneous fission of ^{254}Cf, normalized to $t = 6$ days. The filled and the hollow triangles are the observed and the lower bound of the brightness of the GW170817 kilonova. Data for this plot are taken from [62]

The primary reason behind the possibility of the above discoveries is rather simple: these nuclei generate much larger energy per decay (α or fission) than that from the β-decay of non-actinides. For instance, the α decays of aforementioned actinides with half-lives of days are followed by a sequence of fast α and β decays with much shorter half-lives before reaching stable isotopes. The total released energy in each of these decay chains is $\sim$ 30 MeV. For the case of the fission of ^{254}Cf, it releases $\sim$ 180 MeV per decay. These values are much larger than the typical β-decay energy release of $\lesssim \mathcal{O}(1)$ MeV per nucleus. Moreover, the thermalization efficiencies of

[1] In r-process, ^{225}Ac is actually produced via the β-decay of ^{225}Ra, which has a similar half-life of 14.9 days.

products from the α-decay sequence and fission are typically higher than those from β-decay, where neutrinos and γ-rays can carry a significant part of the energy away without thermalization [89, 101]. Consequently, these decay channels can dominate the energy deposition into the ejecta even with much smaller abundances than the β-decay non-actinide nuclei and leave imprints on kilonova observations. A caution here is that the detailed effects of the excessive heating on the precise spectral evolution of kilonovae at such late times require improved radiation emission modeling during the nebula phase of kilonovae [102, 103]. Future work along this direction is crucial if one would like to convincingly use the late-time kilonova lightcurve to obtain information regarding the presence of actinides or to even constrain the associated theoretical nuclear physics inputs.

Besides the impact of actinide production on kilonova lightcurves, their presence might also contribute to the γ-ray emission from individual BNSM event [101, 104–108] or from old BNSM remnants ($\sim 10^4$–10^6 years old) residing inside the Milky Way [105, 109, 110]. In particular, [109] suggested that if future sub-MeV γ-ray missions can reach a line sensitivity of $\sim 10^{-8}\ \gamma\ \mathrm{cm}^{-2}\ \mathrm{s}^{-1}$, then there is a non-negligible chance ($\sim 10-30\%$) to detect lines from the decay of ^{230}Th with a number fraction of $\sim 10^{-5}-10^{-6}$ per merger in Milky Way's old BNSM remnants. If such lines are detected and the remnant is confirmed to be produced by a past BNSM, it will provide a direct evidence of actinide production in BNSMs. Meanwhile, Ref. [106] found that the γ emissions from fissioning actinides may dominate the smeared spectra above $\gtrsim 3$ MeV during $\sim 10-1000$ days post merger. This would require a Galactic event even for future missions, but can in principle be a potential signature of actinide production in mergers.

4 Actinides in metal-poor stars

Stars with [Fe/H]$\lesssim -2$ are known as very metal-poor (VMP) stars. Low mass VMP stars of $\lesssim 0.9\,M_\odot$ are thought to have formed within ~ 1–2 Gyr from the time of Big Bang and are still alive today. The surface composition of VMP stars provide a direct snapshot of the interstellar medium (ISM) in the early Galaxy. This is particularly important because the abundance patterns of elements in the early Galaxy are thought to be from a few nucleosynthetic events. With regard to r-process, VMP stars that are formed from ISM enriched in r-process ([Ba/Eu]<0), provide a direct measurement of the nucleosynthesis from individual r-process sources. Depending on the level of r-process enrichment, they are classified as r-I ($0.3 \leq$ [Eu/Fe] ≤ 1) and r-II ([Eu/Fe] > 1) stars [135]. Starting with the discovery of the famous r-II star CS 22892-052 [136, 137], a number of r-I and r-II stars have been discovered that have detailed abundance patterns for heavy elements. Remarkably, these stars show

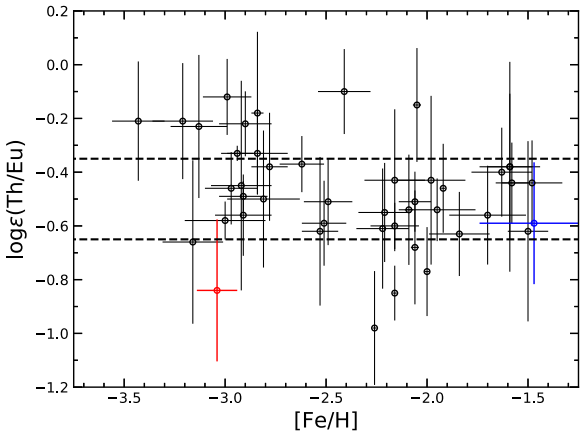

Fig. 5 Observed abundance of Th/Eu in metal-poor stars in the Milky Way (black), Reticulum II (red) and Ursa Minor (blue). Data is generated using the SAGA database [111] and adapted from Refs. [112–134]

an almost identical abundance pattern that agrees well with the Solar r-process pattern from Ba to Pb [33, 34]). However, some of the r-II stars show an enhanced Th abundance (relative to Eu) when compared to the rest of the r-II stars [126]. These are referred to as actinide-boost stars. Figure 5 shows the observed Th/Eu ratio vs [Fe/H] as observed in VMP as well as metal-poor stars. As can be seen for the figure, there is a considerable scatter of up to an order of magnitude in the observed Th/Eu ratio. Despite the large scatter, the definition of stars with "normal" Th/Eu ratio is somewhat subjective due to the considerable 1σ uncertainty of $\gtrsim 0.15$ dex in the observed Th/Eu ratio in individual stars. The horizontal lines shown in Fig. 5 shows the band corresponding to $\log\epsilon(\mathrm{Th/Eu}) = -0.5 \pm 0.15$[2] as adopted recently by Ref. [128] to define "normal" Th/Eu stars. With this definition, there are 3 stars with Th/Eu values that are clearly above the band and 5 more stars that have mean values above -0.35 but still lies within the band when the 1σ error is taken into account. Similarly, there are two stars whose Th/Eu values are clearly below the band and 3 more stars whose mean values are below -0.65 but lie within the band when 1σ uncertainty is taken into account. Regardless of the exact definition of what a normal r-process Th/Eu ratio is, it is clear that the difference in the Th/Eu ratio in stars above and below the band is statistically significant and points to variations in the actinide abundance that is in sharp contrast with the robust pattern seen in elements between the second and third r-process peak.

Refs. [54, 128] investigated whether BNSMs can account for the scattering of the observed $\log\epsilon(\mathrm{Th/Eu})$ discussed above, and found that a proper mixture of low $Y_e \lesssim$

[2] $\log\epsilon(\mathrm{X}) \equiv \log(N_\mathrm{X}/N_\mathrm{H}) + 12$, where N_X and N_H are the number of atoms of element X and hydrogen, respectively. For elements X and Y, $\log\epsilon(\mathrm{X/Y}) = \log\epsilon(\mathrm{X}) - \log\epsilon(\mathrm{Y}) = \log(N_\mathrm{X}/N_\mathrm{Y})$.

0.15 and high Y_e components can easily reproduce the observed range of $\log\epsilon$(Th/Eu). In such a scenario, the low $Y_e \lesssim 0.15$ component may produce $\log\epsilon(\mathrm{Th/Eu}) \gtrsim 0$ and the high $Y_e \gtrsim 0.15$ component plays the role of diluting $\log\epsilon$(Th/Eu). For example, both the FRDM+Möeller03 model and DZ31+Möeller03 model shown in Fig. 2 produce $0 \lesssim \log\epsilon(\mathrm{Th/Eu}) \lesssim 1.0$ for $Y_e \lesssim 0.15$ (taken at $t = 13$ Gyr). Since this value decreases rapidly with increasing $Y_e \gtrsim 0.15$, a dilution factor of $\sim 1-10$ for both cases can lower $\log\epsilon$(Th/Eu) to the observed range shown in Fig. 5. On the other hand, the model FRDM+D3C* only obtains $\log\epsilon(\mathrm{Th/Eu}) \lesssim -0.7$, which appears to be inconsistent with the observations. This may point to the possibility of constraining the β-decay half-lives of exotic neutron-rich heavy nuclei with metal-poor stars. However, given the large uncertainties involved in model predictions and observations, it is too early to draw any definite conclusions.

In addition to the Th (and U) abundances that can be directly used to infer the actinide production in BNSMs, a precise measurement of the abundance of Pb can also provide useful information. This is because most of the non-fissioning actinides produced by *r*-process ultimately decay to Pb isotopes (other than those blocked by Th). In particular, it may be used to constrain the amount of α-decay nuclei relevant for kilonova discussed in Section 3 assuming BNSMs are indeed the sites enriching these stars [94]. Notwithstanding the large theoretical and even larger observational uncertainties associated with the Pb abundance that precludes a definite answer now, it may be worthwhile to examine this in future with improved theoretical understanding as well as better observational data (e.g., [138]).

5 Short-lived radioactive actinides

Radioactive isotopes that have half-lives of a few Myr are called short-lived radioactive isotopes (SLRIs). They provide crucial information about the local enrichment history over the relatively short timescales of their half-lives. Broadly, abundance of SLRIs can be measured in three distinct regimes. The first is the measurement of live SLRIs present in the ISM using γ-ray telescopes that detect the emitted γ-rays following radioactive decay of SLRIs such as ^{26}Al and ^{60}Fe. Such measurements have been used to directly probe ongoing star formation in the Galaxy [139, 140], and can in principle be used to probe the BNSM history as well (see Section 3). On the other hand, live SLRIs that are incident on Earth are eventually deposited at the Earth's deep sea floor which grows over time. Measuring SLRIs in different layers of such sea crusts gives the enrichment history of the local ISM over the last $\sim$10–25 Myrs. Lastly, and remarkably, abundance of SLRIs that were present at the time of the formation of the Solar system can be measured by analyzing the isotopic anomalies in meteorites resulting from the SLRIs decaying to stable daughter isotopes. This can probe the nucleosynthetic events that occurred within a few Myr before the formation of the Solar system.

With regard to *r*-process, the important SLRIs are ^{129}I (half-life of 15.6 Myr) and actinides ^{244}Pu (half-life of 81 Myr) and ^{247}Cm (half-life of 15.7 Myr). In terms of live SLRIs measured in deep sea crusts, ^{244}Pu is particularly important because of its relatively longer half-life. Ref. [41] have shown that the amount of live ^{244}Pu accumulated in deep sea crust over the last 25 Myr can be used to estimate the local ISM density of ^{244}Pu which turns out to be about two orders of magnitude lower than the amount expected from a frequent *r*-process source associated with a regular core-collapse SN. More recent measurements of deep sea crust that correspond to the last $\sim$ 10 Myr also point towards a rare *r*-process source [45]. Interestingly, ^{244}Pu has also been measured in meteorites and has been shown to be present in the early Solar system (ESS) with an abundance of $^{244}\mathrm{Pu}/^{238}\mathrm{U} = (7 \pm 1) \times 10^{-3}$ [141]. Surprisingly, the abundance measured in the ESS corresponds to an ISM density that is $\sim$ two orders of magnitude higher than the value inferred from deep sea measurement. Figure 6a shows the evolution of local ISM ^{244}Pu density with time for two different *r*-process sources with a frequencies of 500 Myr^{-1} and 10 Myr^{-1} using the turbulent gas diffusion prescription used in Ref. [142]. As can bee clearly seen from the figure, an *r*-process source that has a lower frequency is required to account for the ~ 2 orders of magnitude variation in local ^{244}Pu density. This essentially rules out the possibility of a frequent *r*-process source associated with core-collapse SN and points to a rare but prolific source with an upper limit of the inferred occurrence rate of $\lesssim 10\,\mathrm{Myr}^{-1}$ [142], which is consistent with BNSMs or some rare supernovae (SNe) such as the magneto-rotational SNe (MRSNe) [143–145]. In addition to the constraint put by ^{244}Pu ISM density, Ref. [43] showed that the abundance ratio of $^{247}\mathrm{Cm}/^{244}\mathrm{Pu}$ in the ESS can also be used to directly constrain the *r*-process event rate during the formation of the Solar system with a inferred rate of 1–100 Myr^{-1}. Figure 6b shows the corresponding evolution of the $^{247}\mathrm{Cm}/^{244}\mathrm{Pu}$ for the models plotted in Fig. 6a. As can be seen clearly from the figure, an *r*-process source with higher frequency results in $^{247}\mathrm{Cm}/^{244}\mathrm{Pu}$ that is always higher than the measured value in the ESS. On the other hand, a rare *r*-process source of BNSM-type can easily account for the observed value.

The ESS measurement of ^{247}Cm is also particularly interesting when combined with the measurement of ^{129}I. In a recent study by Ref. [44], it was shown that due to the fortuitous coincidence of nearly identical half-lives of

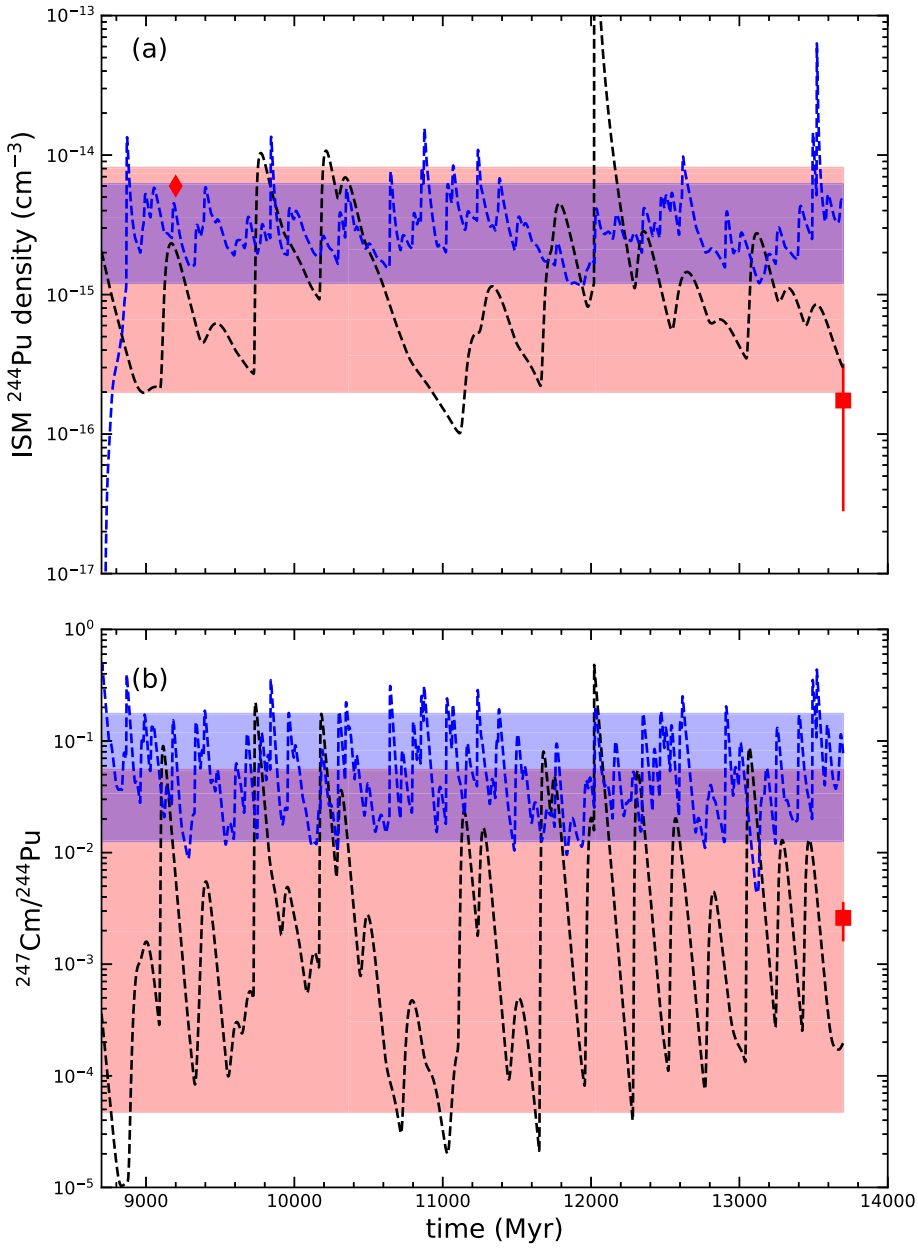

Fig. 6 a Evolution of ^{244}Pu ISM density for *r*-process sources with rates of 10 Myr^{-1} (red) and 500 Myr^{-1} (blue). The shaded regions show the corresponding 90 percentile range. The estimated ^{244}Pu ISM in the ESS (red diamond) is shown along with the estimated local ISM density over the last 25 Myr estimated from earth's crust (red square) [45]. **b** Evolution of the corresponding ^{247}Cm/^{244}Pu ratio along with the measured ratio in the ESS (red square). The shaded regions correspond to the 90 percentile range

these two isotopes that are also almost exclusively produced by *r*-process, the ^{129}I/^{247}Cm ratio stays constant over time and is not sensitive to the typical uncertainties associated with Galactic chemical evolution. Assuming a rare *r*-process source, it was shown that the value of 438 ± 184 measured in the ESS corresponds to the "last" *r*-process event that contributed to the Solar system inventory. Because the ratio ^{129}I/^{247}Cm is particularly sensitive to the neutron richness, this can directly constrain neutron richness of the "last" *r*-process event. It was shown that the measured value in the ESS is consistent with moderately neutron-rich ejecta that are associated with disk winds following BNSMs. On the other hand, the value is inconsistent with both very neutron-rich ejecta that is usually associated with tidally-disrupted ejecta, and mildly neutron-rich ejecta that associated with MRSNe.

A recent study by Ref. [46] has found that the origin of ^{247}Cm and ^{129}I in the ESS is likely more complicated. In particular, when the turbulent gas diffusion prescription is used to model the ^{129}I and ^{247}Cm abundance, it was found that in addition to a major contributing event, at least two more events contribute substantially to the ESS inventory of ^{129}I/^{247}Cm. As an illustration, Fig. 7 shows the comparison between evolution of the ^{129}I/^{247}Cm ratio for one (black) and two (blue) *r*-process sources. In the case with two sources, it is assumed that they are equally frequent and have distinct ^{129}I/^{247}Cm production ratios of 10 and 100. As can be seen clearly from the figure, with two sources, the value of ^{129}I/^{247}Cm not only takes 10 and 100 but also intermediate values for substantial intervals. Thus, the measured value of the ^{129}I/^{247}Cm ratio may not correspond to the production ratios of the individual *r*-process event. Furthermore, it was shown that when the measured values of ^{129}I/^{127}I and ^{247}Cm/^{235}U are taken in to account, the effect is even more dramatic with the major contributor accounting for only ∼50% of the ^{129}I in the ESS. Overall, it was found that it is not possible to put straightforward constraint on the "last" *r*-process source using the measured ESS ratio of ^{129}I/^{247}Cm. Nevertheless, ^{129}I/^{247}Cm can still be used to put important constraints on the nature of *r*-process sources that were operating during the formation of the Solar system. In particular, an *r*-process source that is primarily composed of low Y_e ejecta as a major source of *r*-process is highly disfavored.

6 Conclusion

In this short review article, we have discussed several aspects related to actinide production in *r*-process sites and particularly in BNSMs. First, we reviewed the general condition ($Y_e \lesssim 0.2$) for actinide production via *r*-process in typical neutron star merger outflows. We then demonstrated with simple examples the impact of yet-uncertain nuclear physics inputs (including masses, β-decay half-lives, and fission) on actinide production relevant for kilonova observations. Mass models that predict steeper drops of neutron separation energies around $Z \sim 78$ and $N \sim 150$ generally lead to an *r*-process path closer to the stability and permit higher actinide yields around $A \sim 230$. For β-decays, a mass model that predicts longer half-lives for actinides directly leads to a smaller amount of actinide production. Nuclear fission predictions directly affect the amount of actinides that survive against fission for $A \gtrsim 250$, and indirectly influence $A \sim 220 - 230$ through their impact on post freeze-out abundance of neutrons.

We further reviewed the recent findings regarding the impact of actinide production in BNSM outflows on kilonova lightcurves. Both the α-decay nuclei (^{222}Rn, ^{224}Ra, ^{223}Ra and ^{225}Ac) and the spontaneous fission nucleus ^{254}Cf can dominate the radioactive heating for kilonovae at late times ($\gtrsim$ 10 days) even with subdominant yields, due to their larger energy release per nucleus than β decays. Detailed late-time observations of future kilonovae, together with improved theoretical modeling of radiation at relevant times can possibly probe the presence of actinides in BNSM outflows. Moreover, the amount of actinides produced in BNSMs may also leave imprints on γ-ray emission for live events or for older remnants ($\sim 10^4$–10^6 years old) in our Milky Way, which may be probed by the next generation MeV γ-ray missions.

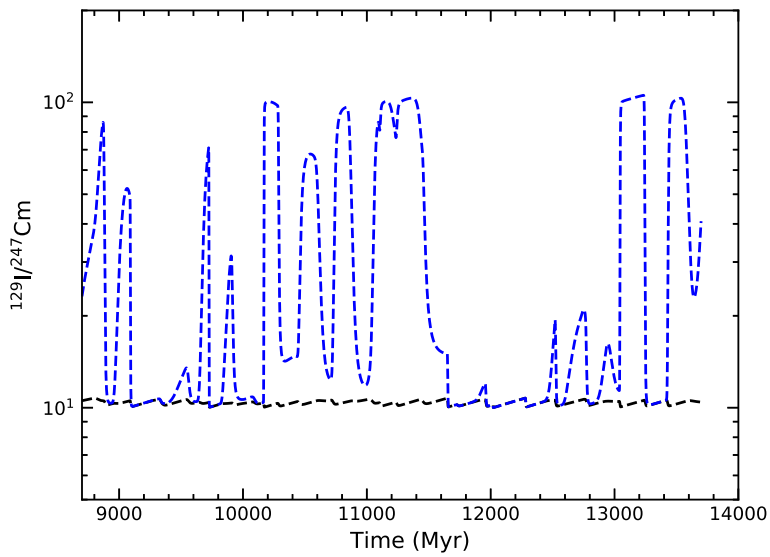

Fig. 7 Evolution of ^{129}I/^{247}Cm: One *r*-process source with ^{129}I/^{247}Cm production ratio of 10 is plotted in black. The case where there are two equally frequent sources with ^{129}I/^{247}Cm production ratios of 10 and 100, respectively, is shown in blue. In both cases the total rate of *r*-process events is 10 Myr^{-1}

Beyond the detection of electromagnetic signatures that may be realized in future, we also discussed the implications of actinide production in mergers from clues obtained with abundances observed in VMP stars as well as with the SLRIs measured in deep-sea crusts and meteorites. The observed VMP stars show a large scatter of Th abundances by $\sim$ a factor of 10 relative to the Eu abundances (classified as actinide-boost, normal, and actinide-poor). This scatter can be explained by a mixture of high and low Y_e components of BNSM ejecta. However, nuclear physics models that predict low Th yields are in tension with actinide boost stars, and may be constrained with improved observational uncertainties, if these stars were indeed enriched by BNSMs. Besides, better determination of the abundance of Pb in VMP stars in future can also offer insights into the amount of α-decay actinides production during BNSMs.

With regard to SLRIs, we reviewed the important conclusions derived in literature that measurements of ^{244}Pu and ^{247}Cm in ESS and in Earth's deep-sea crust suggest they were dominantly produced by a rare and prolific BNSM-like source with an occurrence frequency of $\sim$ 10 Myr in Milky Way, instead of a more frequent source like typical core-collapse supernovae. Furthermore, we discussed recent findings on the implication of the measured abundance ratio of SLRIs ^{247}Cm to ^{129}I (both have almost identical half-lives) in the ESS, as inferred from meteorites, on the *r*-process condition in BNSMs. If the ratio measured in the ESS ratio was from a single "last" polluting *r*-process event, then a moderately neutron-rich condition (similar to the BNSM accretion disk outflow) is preferred. However, it remains likely that multiple events contributed to this ratio such that a direct inference deduced from single event assumption is not valid. In this case, this measurement still suggests that an *r*-process source dominantly consisting of low Y_e material as the major source of *r*-process is disfavored.

In summary, in recent years, tremendous observational efforts in several directions have helped to gain crucial insights in to *r*-process and indicates BNSMs as the likely source. This is also consistent with current theoretical predictions although a clear answer, particularly regarding the exact level of neutron richness and associated actinide production, is still lacking. In order to reach a definitive conclusion, further improvements are required in theoretical predictions combined with additional observational data. It is hopeful that with all the probes summarized in the review, and potentially other new ideas, this question will be fully answered in the coming decades.

Acknowledgements
The authors are grateful for the fruitful collaboration with Jennifer Barnes, Samuel Giuliani, Gabriel Martìnez-Pinedo, and Brian Metzger leading to works relevant to this paper, and thank Benoit Côte, Kenta Hotokezaka, Yong-Zhong Qian, Friedel Thielemann, and Zhen Yuan for insightful discussions and exchanges over the past few years.

Authors' contributions
MRW and PB contributed equally to this work. Both authors read and approved the final manuscript.

Funding
This work was partially supported by the Ministry of Science and Technology, Taiwan under Grant No. 110-2112-M-001-050, the Academia Sinica under Project No. AS-CDA-109-M11, and the Physics Division, National Center for Theoretical Sciences, Taiwan.

Availability of data and materials
All data contained in this work are available on reasonable request.

Declarations

Ethics approval and consent to participate
Not Applicable.

Consent for publication
Not Applicable.

Competing interests
The authors declare that they have no competing interests.

Author details
[1]Institute of Physics, Academia Sinica, Taipei 11529, Taiwan. [2]Institute of Astronomy and Astrophysics, Academia Sinica, Taipei 10617, Taiwan. [3]Department of Physics, Indian Institute of Technology Palakkad, Kerala 678558, India.

Received: 24 May 2022 Accepted: 19 June 2022
Published online: 15 July 2022

References

1. B. P. Abbott, R. Abbott, T. D. Abbott, F. Acernese, K. Ackley, C. Adams, T. Adams, P. Addesso, R. X. Adhikari, V. B. Adya, C. Affeldt, M. Afrough, B. Agarwal, M. Agathos, K. Agatsuma, N. Aggarwal, O. D. Aguiar, L. Aiello, A. Ain, M. Bailes, P. T. Baker, F. Baldaccini, G. Ballardin, S. W. Ballmer, S. Banagiri, J. C. Barayoga, S. E. Barclay, B. C. Barish, D. Barker, K. Barkett, F. Barone, B. Barr, L. Barsotti, M. Barsuglia, D. Barta, S. D. Barthelmy, J. Bartlett, I. Bartos, R. Bassiri, A. Basti, J. C. Batch, M. Bawaj, GW170817: Observation of Gravitational Waves from a Binary Neutron Star Inspiral. Phys. Rev. Lett. **119**(16), 161101 (2017). arXiv:1710.05832. [gr-qc]. https://doi.org/10.1103/PhysRevLett.119.161101
2. B. P. Abbott, R. Abbott, T. D. Abbott, F. Acernese, K. Ackley, C. Adams, T. Adams, P. Addesso, R. X. Adhikari, V. B. Adya, C. Affeldt, M. Afrough, B. Agarwal, M. Agathos, K. Agatsuma, N. Aggarwal, O. D. Aguiar, L. Aiello, A. Ain, P. Ajith, B. Allen, G. Allen, A. Allocca, P. A. Altin, A. Amato, A. Ananyeva, S. B. Anderson, W. G. Anderson, S. V. Angelova, S. Antier, S. Appert, K. Arai, M. C. Araya, J. S. Areeda, N. Arnaud, K. G. Arun, S. Ascenzi, G. Ashton, M. Ast, S. M. Aston, P. Astone. Astrophys. J. Lett. **848**(2), 12 (2017). arXiv:1710.05833. https://doi.org/10.3847/2041-8213/aa91c9
3. B. D. Metzger, Kilonovae. Living Rev. Rel. **23**(1), 1 (2020). arXiv:1910.01617. https://doi.org/10.1007/s41114-019-0024-0
4. E. Nakar, The electromagnetic counterparts of compact binary mergers. Phys. Rept. **886**, 1–84 (2020). arXiv:1912.05659. https://doi.org/10.1016/j.physrep.2020.08.008
5. M. Shibata, K. Hotokezaka, Merger and Mass Ejection of Neutron-Star Binaries. Ann. Rev. Nucl. Part. Sci. **69**, 41–64 (2019). arXiv:1908.02350. https://doi.org/10.1146/annurev-nucl-101918-023625
6. R. Margutti, R. Chornock, First Multimessenger Observations of a Neutron Star Merger. Ann. Rev. Astron. Astrophys. **59**, 155–202 (2021). arXiv:2012.04810. https://doi.org/10.1146/annurev-astro-112420-030742
7. A. Perego, F.-K. Thielemann, G. Cescutti, *r-Process Nucleosynthesis from Compact Binary Mergers*, (2021). https://doi.org/10.1007/978-981-15-4702-7_13-1
8. E. Annala, T. Gorda, A. Kurkela, A. Vuorinen, Gravitational-wave constraints on the neutron-star-matter Equation of State. Phys. Rev. Lett. **120**(17), 172703 (2018). arXiv:1711.02644. https://doi.org/10.1103/PhysRevLett.120.172703

9. B. Margalit, B. D. Metzger, Constraining the Maximum Mass of Neutron Stars From Multi-Messenger Observations of GW170817. Astrophys. J. Lett. **850**(2), 19 (2017). arXiv:1710.05938. https://doi.org/10.3847/2041-8213/aa991c
10. L. Rezzolla, E. R. Most, L. R. Weih, Using gravitational-wave observations and quasi-universal relations to constrain the maximum mass of neutron stars. Astrophys. J. Lett. **852**(2), 25 (2018). arXiv:1711.00314. https://doi.org/10.3847/2041-8213/aaa401
11. A. Bauswein, O. Just, H.-T. Janka, N. Stergioulas, Neutron-star radius constraints from GW170817 and future detections. Astrophys. J. Lett. **850**(2), 34 (2017). arXiv:1710.06843. https://doi.org/10.3847/2041-8213/aa9994
12. D. Radice, A. Perego, F. Zappa, S. Bernuzzi, GW170817: Joint Constraint on the Neutron Star Equation of State from Multimessenger Observations. Astrophys. J. Lett. **852**(2), 29 (2018). arXiv:1711.03647. https://doi.org/10.3847/2041-8213/aaa402
13. H.-Y. Chen, M. Fishbach, D. E. Holz, A two per cent Hubble constant measurement from standard sirens within five years. Nature. **562**(7728), 545–547 (2018). arXiv:1712.06531. [astro-ph.CO]. https://doi.org/10.1038/s41586-018-0606-0
14. V. Paschalidis, K. Yagi, D. Alvarez-Castillo, D. B. Blaschke, A. Sedrakian, Implications from GW170817 and I-Love-Q relations for relativistic hybrid stars. Phys. Rev. D. **97**(8), 084038 (2018). arXiv:1712.00451. https://doi.org/10.1103/PhysRevD.97.084038
15. K. Hotokezaka, E. Nakar, O. Gottlieb, S. Nissanke, K. Masuda, G. Hallinan, K. P. Mooley, A. T. Deller, A Hubble constant measurement from superluminal motion of the jet in GW170817. Nature Astron. **3**(10), 940–944 (2019). arXiv:1806.10596. [astro-ph.CO]. https://doi.org/10.1038/s41550-019-0820-1
16. T. Malik, N. Alam, M. Fortin, C. Providência, B. K. Agrawal, T. K. Jha, B. Kumar, S. K. Patra, GW170817: constraining the nuclear matter equation of state from the neutron star tidal deformability. Phys. Rev. C. **98**(3), 035804 (2018). arXiv:1805.11963. https://doi.org/10.1103/PhysRevC.98.035804
17. S. De, D. Finstad, J. M. Lattimer, D. A. Brown, E. Berger, C. M. Biwer, Tidal Deformabilities and Radii of Neutron Stars from the Observation of GW170817. Phys. Rev. Lett. **121**(9), 091102 (2018). arXiv:1804.08583. https://doi.org/10.1103/PhysRevLett.121.091102. [Erratum: Phys.Rev.Lett. 121, 259902 year=2018]
18. C. D. Capano, I. Tews, S. M. Brown, B. Margalit, S. De, S. Kumar, D. A. Brown, B. Krishnan, S. Reddy, Stringent constraints on neutron-star radii from multimessenger observations and nuclear theory. Nature Astron. **4**(6), 625–632 (2020). arXiv:1908.10352. https://doi.org/10.1038/s41550-020-1014-6
19. T. Dietrich, M. W. Coughlin, P. T. H. Pang, M. Bulla, J. Heinzel, L. Issa, I. Tews, S. Antier, Multimessenger constraints on the neutron-star equation of state and the Hubble constant. Science. **370**(6523), 1450–1453 (2020). arXiv:2002.11355. https://doi.org/10.1126/science.abb4317
20. T. Kojo, QCD equations of state and speed of sound in neutron stars. AAPPS Bull. **31**(1), 11 (2021). arXiv:2011.10940. https://doi.org/10.1007/s43673-021-00011-6
21. Y.-L. Ma, M. Rho, Topology change, emergent symmetries and compact star matter. AAPPS Bull. **31**(1), 16 (2021). arXiv:2103.00744. https://doi.org/10.1007/s43673-021-00016-1
22. A. A. Aziz, *et al*, Progress in nuclear astrophysics of east and southeast Asia. AAPPS Bull. **31**(1), 18 (2021). arXiv:2108.03814. [nucl-ex]. https://doi.org/10.1007/s43673-021-00018-z
23. D. Kasen, B. Metzger, J. Barnes, E. Quataert, E. Ramirez-Ruiz, Origin of the heavy elements in binary neutron-star mergers from a gravitational-wave event. Nature. **551**, 80–84 (2017). arXiv:1710.05463. https://doi.org/10.1038/nature24453
24. M. R. Drout, A. L. Piro, B. J. Shappee, C. D. Kilpatrick, J. D. Simon, C. Contreras, D. A. Coulter, R. J. Foley, M. R. Siebert, N. Morrell, K. Boutsia, F. Di Mille, T. W.-S. Holoien, D. Kasen, J. A. Kollmeier, B. F. Madore, A. J. Monson, A. Murguia-Berthier, Y.-C. Pan, J. X. Prochaska, E. Ramirez-Ruiz, A. Rest, C. Adams, K. Alatalo, E. Bañados, J. Baughman, T. C. Beers, R. A. Bernstein, T. Bitsakis, A. Campillay, T. T. Hansen, C. R. Higgs, A. P. Ji, G. Maravelias, J. L. Marshall, C. Moni Bidin, J. L. Prieto, K. C. Rasmussen, C. Rojas-Bravo, A. L. Strom, N. Ulloa, J. Vargas-González, Z. Wan, D. D. Whitten, Light curves of the neutron star merger GW170817/SSS17a: Implications for r-process nucleosynthesis. Science. **358**(6370), 1570–1574 (2017). arXiv:1710.05443. https://doi.org/10.1126/science.aaq0049
25. P. S. Cowperthwaite, E. Berger, V. A. Villar, B. D. Metzger, M. Nicholl, R. Chornock, P. K. Blanchard, W. Fong, R. Margutti, M. Soares-Santos, K. D. Alexander, S. Allam, J. Annis, D. Brout, D. A. Brown, R. E. Butler, H.-Y. Chen, H. T. Diehl, Z. Doctor, M. R. Drout, T. Eftekhari, B. Farr, D. A. Finley, R. J. Foley, J. A. Frieman, C. L. Fryer, J. García-Bellido, M. S. S. Gill, J. Guillochon, K. Herner, D. E. Holz, D. Kasen, R. Kessler, J. Marriner, T. Matheson, J. E. H. Neilsen, E. Quataert, A. Palmese, A. Rest, M. Sako, D. M. Scolnic, N. Smith, D. L. Tucker, P. K. G. Williams, E. Balbinot, J. L. Carlin, E. R. Cook, F. Durret, T. S. Li, P. A. A. Lopes, A. C. C. Lourenço, J. L. Marshall, G. E. Medina, J. Muir, R. R. Muñoz, M. Sauseda, D. J. Schlegel, L. F. Secco, A. K. Vivas, W. Wester, A. Zenteno, Y. Zhang, T. M. C. Abbott, M. Banerji, K. Bechtol, A. Benoit-Lévy, E. Bertin, E. Buckley-Geer, D. L. Burke, D. Capozzi, A. Carnero Rosell, M. Carrasco Kind, F. J. Castander, M. Crocce, C. E. Cunha, C. B. D'Andrea, L. N. da Costa, C. Davis, D. L. DePoy, S. Desai, J. P. Dietrich, A. Drlica-Wagner, T. F. Eifler, A. E. Evrard, E. Fernand ez, B. Flaugher, P. Fosalba, E. Gaztanaga, D. W. Gerdes, T. Giannantonio, D. A. Goldstein, D. Gruen, R. A. Gruendl, G. Gutierrez, K. Honscheid, B. Jain, D. J. James, T. Jeltema, M. W. G. Johnson, M. D. Johnson, S. Kent, E. Krause, R. Kron, K. Kuehn, N. Nuropatkin, O. Lahav, M. Lima, H. Lin, M. A. G. Maia, M. March, P. Martini, R. G. McMahon, F. Menanteau, C. J. Miller, R. Miquel, J. J. Mohr, E. Neilsen, R. C. Nichol, R. L. C. Ogando, A. A. Plazas, N. Roe, A. K. Romer, A. Roodman, E. S. Rykoff, E. Sanchez, V. Scarpine, R. Schindler, M. Schubnell, I. Sevilla-Noarbe, M. Smith, R. C. Smith, F. Sobreira, E. Suchyta, M. E. C. Swanson, G. Tarle, D. Thomas, R. C. Thomas, M. A. Troxel, V. Vikram, A. R. Walker, R. H. Wechsler, J. Weller, B. Yanny, J. Zuntz, The Electromagnetic Counterpart of the Binary Neutron Star Merger LIGO/Virgo GW170817. II. UV, Optical, and Near-infrared Light Curves and Comparison to Kilonova Models. Astrophys. J. Lett. **848**(2), 17 (2017). arXiv:1710.05840. https://doi.org/10.3847/2041-8213/aa8fc7
26. V. A. Villar, J. Guillochon, E. Berger, B. D. Metzger, P. S. Cowperthwaite, M. Nicholl, K. D. Alexander, P. K. Blanchard, R. Chornock, T. Eftekhari, W. Fong, R. Margutti, P. K. G. Williams, The Combined Ultraviolet, Optical, and Near-infrared Light Curves of the Kilonova Associated with the Binary Neutron Star Merger GW170817: Unified Data Set, Analytic Models, and Physical Implications. Astrophys. J. Lett. **851**, 21 (2017). arXiv:1710.11576. https://doi.org/10.3847/2041-8213/aa9c84
27. K. Kawaguchi, M. Shibata, M. Tanaka, Radiative Transfer Simulation for the Optical and Near-infrared Electromagnetic Counterparts to GW170817. Astrophys. J. Lett. **865**, 21 (2018). arXiv:1806.04088. https://doi.org/10.3847/2041-8213/aade02
28. D. Watson, *et al*, Identification of strontium in the merger of two neutron stars. Nature. **574**(7779), 497–500 (2019). arXiv:1910.10510. https://doi.org/10.1038/s41586-019-1676-3
29. N. Domoto, M. Tanaka, S. Wanajo, K. Kawaguchi, Signatures of r-process elements in kilonova spectra. Astrophys. J. **913**(1), 26 (2021). arXiv:2103.15284. https://doi.org/10.3847/1538-4357/abf358
30. J. H. Gillanders, M. McCann, S. A. Sim, S. A. S. S. J. Smartt, C. P. Ballance, Constraints on the presence of platinum and gold in the spectra of the kilonova AT2017gfo. Mon. Not. Roy. Astron. Soc. **506**(3), 3560–3577 (2021). arXiv:2101.08271. https://doi.org/10.1093/mnras/stab1861
31. A. Perego, *et al*, Production of Very Light Elements and Strontium in the Early Ejecta of Neutron Star Mergers. Astrophys. J. **925**(1), 22 (2022). arXiv:2009.08988. https://doi.org/10.3847/1538-4357/ac3751
32. M. M. Kasliwal, *et al*, Spitzer mid-infrared detections of neutron star merger GW170817 suggests synthesis of the heaviest elements. Mon. Not. Roy. Astron. Soc. **510**(1), 7–12 (2022). arXiv:1812.08708. https://doi.org/10.1093/mnrasl/slz007
33. C. Sneden, J. J. Cowan, R. Gallino, Neutron-capture elements in the early galaxy,. Annu. Rev. Astron. Astrophys. **46**, 241–288 (2008). https://doi.org/10.1146/annurev.astro.46.060407.145207
34. J. J. Cowan, C. Sneden, J. E. Lawler, A. Aprahamian, M. Wiescher, K. Langanke, G. Martínez-Pinedo, F.-K. Thielemann, Origin of the heaviest elements: The rapid neutron-capture process. Rev. Mod. Phys. **93**(1), 015002 (2021). arXiv:1901.01410. https://doi.org/10.1103/RevModPhys.93.015002
35. W. A. Fowler, F. Hoyle, Nuclear cosmochronology. Annals of Physics. **10**(2), 280–302 (1960). https://doi.org/10.1016/0003-4916(60)90025-7
36. D. N. Schramm, G. J. Wasserburg, Nucleochronologies and the Mean Age of the Elements. Astrophys. J. **162**, 57 (1970). https://doi.org/10.1086/150634

37. J. J. Cowan, F.-K. Thielemann, J. W. Truran, The R-process and nucleochronology. Phys. Rept. **208**(4-5), 267–394 (1991). https://doi.org/10.1016/0370-1573(91)90070-3
38. B. S. Meyer, J. W. Truran, Nucleocosmochronology. Physics Reports. **333-334**, 1–11 (2000). https://doi.org/10.1016/S0370-1573(00)00012-0
39. I. V. Panov, Y. S. Lutostansky, M. Eichler, F. K. Thielemann, Determination of the Galaxy age by the method of uranium–thorium–plutonium isotopic ratios. Phys. Atom. Nucl. **80**(4), 657–665 (2017). https://doi.org/10.1134/S1063778817040202
40. X. H. Wu, P. W. Zhao, S. Q. Zhang, J. Meng, High-precision nuclear chronometer for the cosmos (2021). https://doi.org/10.48550/arXiv.2108.06104
41. A. Wallner, T. Faestermann, J. Feige, C. Feldstein, K. Knie, G. Korschinek, W. Kutschera, A. Ofan, M. Paul, F. Quinto, et al., Abundance of live 244pu in deep-sea reservoirs on earth points to rarity of actinide nucleosynthesis. Nat. Commun. **6**(1) (2015). https://doi.org/10.1038/ncomms6956
42. K. Hotokezaka, T. Piran, M. Paul, Short-lived ^{244}Pu points to compact binary mergers as sites for heavy r-process nucleosynthesis. Nature Physics. **11**(12), 1042 (2015). arXiv:1510.00711. https://doi.org/10.1038/nphys3574
43. I. Bartos, S. Marka, A nearby neutron-star merger explains the actinide abundances in the early Solar System. Nature. **569**(7754), 85–88 (2019). https://doi.org/10.1038/s41586-019-1113-7
44. B. Côté, M. Eichler, A. Yagüe López, N. Vassh, M. R. Mumpower, B. Világos, B. Soós, A. Arcones, T. M. Sprouse, R. Surman, M. Pignatari, M. K. Pető, B. Wehmeyer, T. Rauscher, M. Lugaro, ^{129}I and ^{247}Cm in meteorites constrain the last astrophysical source of solar r-process elements. Science. **371**(6532), 945–948 (2021). arXiv:2006.04833. https://doi.org/10.1126/science.aba1111
45. A. Wallner, M. B. Froehlich, M. A. C. Hotchkis, N. Kinoshita, M. Paul, M. Martschini, S. Pavetich, S. G. Tims, N. Kivel, D. Schumann, M. Honda, H. Matsuzaki, T. Yamagata, ^{60}Fe and ^{244}Pu deposited on Earth constrain the r-process yields of recent nearby supernovae. Science. **372**(6543), 742–745 (2021). https://doi.org/10.1126/science.aax3972
46. P. Banerjee, M.-R. Wu, J. S K, Constraints on r-process nucleosynthesis from ^{129}I and ^{247}Cm in the early Solar system. Mon. Not. Roy. Astron. Soc. **512**(4), 4948–4960 (2022). arXiv:2110.05449. [astro-ph.GA]. https://doi.org/10.1093/mnras/stac318
47. S. Goriely, A. Bauswein, H.-T. Janka, r-process Nucleosynthesis in Dynamically Ejected Matter of Neutron Star Mergers. Astrophys. J. Lett. **738**(2), 32 (2011). arXiv:1107.0899. https://doi.org/10.1088/2041-8205/738/2/L32
48. O. Korobkin, S. Rosswog, A. Arcones, C. Winteler, On the astrophysical robustness of the neutron star merger r-process. Mon. Not. Roy. Astron. Soc. **426**(3), 1940–1949 (2012). arXiv:1206.2379. https://doi.org/10.1111/j.1365-2966.2012.21859.x
49. S. Wanajo, Y. Sekiguchi, N. Nishimura, K. Kiuchi, K. Kyutoku, M. Shibata, Production of all the r-process nuclides in the dynamical ejecta of neutron star mergers. Astrophys. J. Lett. **789**, 39 (2014). arXiv:1402.7317. https://doi.org/10.1088/2041-8205/789/2/L39
50. O. Just, A. Bauswein, R. A. Pulpillo, S. Goriely, H.-T. Janka, Comprehensive nucleosynthesis analysis for ejecta of compact binary mergers. Mon. Not. Roy. Astron. Soc. **448**(1), 541–567 (2015). arXiv:1406.2687. https://doi.org/10.1093/mnras/stv009
51. J. Lippuner, L. F. Roberts, r-Process Lanthanide Production and Heating Rates in Kilonovae. Astrophys. J. **815**(2), 82 (2015). arXiv:1508.03133. https://doi.org/10.1088/0004-637X/815/2/82
52. M.-R. Wu, R. Fernández, G. Martínez-Pinedo, B. D. Metzger, Production of the entire range of r-process nuclides by black hole accretion disc outflows from neutron star mergers. Mon. Not. Roy. Astron. Soc. **463**(3), 2323–2334 (2016). arXiv:1607.05290. https://doi.org/10.1093/mnras/stw2156
53. D. M. Siegel, B. D. Metzger, Three-Dimensional General-Relativistic Magnetohydrodynamic Simulations of Remnant Accretion Disks from Neutron Star Mergers: Outflows and r-Process Nucleosynthesis. Phys. Rev. Lett. **119**(23), 231102 (2017). arXiv:1705.05473. https://doi.org/10.1103/PhysRevLett.119.231102
54. E. M. Holmbeck, R. Surman, T. M. Sprouse, M. R. Mumpower, N. Vassh, T. C. Beers, T. Kawano, Actinide Production in the Neutron-rich Ejecta of a Neutron Star Merger. Astrophys. J. **870**(1), 23 (2019). arXiv:1807.06662. https://doi.org/10.3847/1538-4357/aaefef
55. E. M. Holmbeck, A. Frebel, G. C. McLaughlin, M. R. Mumpower, T. M. Sprouse, R. Surman, Actinide-rich and Actinide-poor r-Process Enhanced Metal-Poor Stars do not Require Separate r-Process Progenitors (2019). arXiv:1904.02139. https://doi.org/10.3847/1538-4357/ab2a01
56. M. Eichler, W. Sayar, A. Arcones, T. Rauscher, Probing the production of actinides under different r-process conditions. Astrophys. J. **879**(1), 47 (2019). arXiv:1904.07013. https://doi.org/10.3847/1538-4357/ab24cf
57. R. Fernández, F. Foucart, J. Lippuner, The landscape of disc outflows from black hole–neutron star mergers. Mon. Not. Roy. Astron. Soc. **497**(3), 3221–3233 (2020). arXiv:2005.14208. https://doi.org/10.1093/mnras/staa2209
58. V. Nedora, S. Bernuzzi, D. Radice, B. Daszuta, A. Endrizzi, A. Perego, A. Prakash, M. Safarzadeh, F. Schianchi, D. Logoteta, Numerical Relativity Simulations of the Neutron Star Merger GW170817: Long-Term Remnant Evolutions, Winds, Remnant Disks, and Nucleosynthesis. Astrophys. J. **906**(2), 98 (2021). arXiv:2008.04333. https://doi.org/10.3847/1538-4357/abc9be
59. I. Kullmann, S. Goriely, O. Just, R. Ardevol-Pulpillo, A. Bauswein, H.-T. Janka, Dynamical ejecta of neutron star mergers with nucleonic weak processes I: nucleosynthesis. Mon. Not. Roy. Astron. Soc. **510**(2), 2804–2819 (2022). arXiv:2109.02509. https://doi.org/10.1093/mnras/stab3393
60. S. Fujibayashi, K. Kiuchi, S. Wanajo, K. Kyutoku, Y. Sekiguchi, M. Shibata, Comprehensive study on the mass ejection and nucleosynthesis in the binary neutron star mergers leaving short-lived massive neutron stars (2022). https://doi.org/10.48550/arXiv.2205.05557
61. S. E. Woosley, R. D. Hoffman, The alpha -Process and the r-Process. Astrophys. J. **395**, 202 (1992). https://doi.org/10.1086/171644
62. M.-R. Wu, J. Barnes, G. Martínez-Pinedo, B. D. Metzger, Fingerprints of Heavy-Element Nucleosynthesis in the Late-Time Lightcurves of Kilonovae. Phys. Rev. Lett. **122**(6), 062701 (2019). arXiv:1808.10459. https://doi.org/10.1103/PhysRevLett.122.062701
63. S. Goriely, B. Clerbaux, Uncertainties in the th cosmochronometry. Astron. Astrophys. **346**, 798 (1999). https://doi.org/10.48550/arXiv.astro-ph/9904409
64. I. V. Panov, I. Y. Korneev, G. Martinez-Pinedo, F. K. Thielemann, Influence of spontaneous fission rates on the yields of superheavy elements in the r-process. Astron. Lett. **39**, 150–160 (2013). https://doi.org/10.1134/S1063773713030043
65. M. Eichler, *et al*, The Role of Fission in Neutron Star Mergers and its Impact on the r-Process Peaks. Astrophys. J. **808**(1), 30 (2015). arXiv:1411.0974. https://doi.org/10.1088/0004-637X/808/1/30
66. J. d. J. Mendoza-Temis, M.-R. Wu, K. Langanke, G. Martínez-Pinedo, A. Bauswein, H.-T. Janka, Nuclear robustness of the r process in neutron-star mergers. Phys. Rev. C. **92**(5), 055805 (2015). arXiv:1409.6135. https://doi.org/10.1103/PhysRevC.92.055805
67. S. Goriely, H.-T. Janka, Solar r-process-constrained actinide production in neutrino-driven winds of supernovae. Mon. Not. Roy. Astron. Soc. **459**(4), 4174–4182 (2016). arXiv:1603.04282. https://doi.org/10.1093/mnras/stw946
68. N. Vassh, *et al*, Using excitation-energy dependent fission yields to identify key fissioning nuclei in r-process nucleosynthesis. J. Phys. G. **46**(6), 065202 (2019). arXiv:1810.08133. https://doi.org/10.1088/1361-6471/ab0bea
69. Y. Zhu, *et al*, Californium-254 and kilonova light curves. Astrophys. J. Lett. **863**(2), 23 (2018). arXiv:1806.09724. https://doi.org/10.3847/2041-8213/aad5de
70. S. A. Giuliani, G. Martínez-Pinedo, M.-R. Wu, L. M. Robledo, Fission and the r -process nucleosynthesis of translead nuclei in neutron star mergers. Phys. Rev. C. **102**(4), 045804 (2020). arXiv:1904.03733. https://doi.org/10.1103/PhysRevC.102.045804
71. Y. L. Zhu, K. Lund, J. Barnes, T. M. Sprouse, N. Vassh, G. C. McLaughlin, M. R. Mumpower, R. Surman, Modeling Kilonova Light Curves: Dependence on Nuclear Inputs. Astrophys. J. **906**(2), 94 (2021). arXiv:2010.03668. https://doi.org/10.3847/1538-4357/abc69e
72. J.-F. Lemaître, S. Goriely, A. Bauswein, H.-T. Janka, Fission fragment distributions and their impact on the r-process nucleosynthesis in neutron star mergers. Phys. Rev. C. **103**(2), 025806 (2021). arXiv:2102.03686. https://doi.org/10.1103/PhysRevC.103.025806
73. P. Moller, J. R. Nix, W. D. Myers, W. J. Swiatecki, Nuclear ground state masses and deformations. Atom. Data Nucl. Data Tabl. **59**, 185–381 (1995). arXiv:nucl-th/9308022. https://doi.org/10.1006/adnd.1995.1002

74. J. Duflo, A. P. Zuker, Microscopic mass formulae. Phys. Rev. C. **52**, 23 (1995). arXiv:nucl-th/9505011. https://doi.org/10.1103/PhysRevC.52.R23
75. P. Moller, B. Pfeiffer, K.-L. Kratz, New calculations of gross beta decay properties for astrophysical applications: Speeding up the classical r process. Phys. Rev. C. **67**, 055802 (2003). https://doi.org/10.1103/PhysRevC.67.055802
76. T. Marketin, L. Huther, G. Martínez-Pinedo, Large-scale evaluation of β-decay rates of r-process nuclei with the inclusion of first-forbidden transitions. Phys. Rev. C. **93**(2), 025805 (2016). arXiv:1507.07442. https://doi.org/10.1103/PhysRevC.93.025805
77. M. Arnould, S. Goriely, K. Takahashi, The r-process of stellar nucleosynthesis: Astrophysics and nuclear physics achievements and mysteries. Phys. Rept. **450**(4-6), 97–213 (2007). arXiv:0705.4512. https://doi.org/10.1016/j.physrep.2007.06.002
78. K.-L. Kratz, J.-P. Bitouzet, F.-K. Thielemann, P. Moeller, B. Pfeiffer, Isotopic r-Process Abundances and Nuclear Structure Far from Stability: Implications for the r-Process Mechanism. Astrophys. J. **403**, 216 (1993). https://doi.org/10.1086/172196
79. D. Peña-Arteaga, S. Goriely, N. Chamel, Relativistic mean-field mass models. Eur. Phys. J. A. **52**(10), 320 (2016). https://doi.org/10.1140/epja/i2016-16320-x
80. D. E. Ward, B. G. Carlsson, P. Möller, S. Åberg, Global microscopic calculations of odd-odd nuclei. Phys. Rev. C. **100**(3), 034301 (2019). https://doi.org/10.1103/PhysRevC.100.034301
81. M. Bender, *et al*, Future of Nuclear Fission Theory. J. Phys. G. **47**(11), 113002 (2020). arXiv:2005.10216. https://doi.org/10.1088/1361-6471/abab4f
82. J. Meng, P. Zhao, Relativistic density functional theory in nuclear physics. AAPPS Bull. **31**(1), 2 (2021). https://doi.org/10.1007/s43673-021-00001-8
83. F. Minato, T. Marketin, N. Paar, β-delayed neutron-emission and fission calculations within relativistic quasiparticle random-phase approximation and a statistical model. Phys. Rev. C. **104**(4), 044321 (2021). https://doi.org/10.1103/PhysRevC.104.044321
84. M. R. Mumpower, T. M. Sprouse, A. E. Lovell, A. T. Mohan, Physically Interpretable Machine Learning for nuclear masses (2022). https://doi.org/10.48550/arXiv.2203.10594
85. L.-X. Li, B. Paczynski, Transient events from neutron star mergers. Astrophys. J. Lett. **507**, 59 (1998). arXiv:astro-ph/9807272. https://doi.org/10.1086/311680
86. B. D. Metzger, G. Martinez-Pinedo, S. Darbha, E. Quataert, A. Arcones, D. Kasen, R. Thomas, P. Nugent, I. V. Panov, N. T. Zinner, Electromagnetic Counterparts of Compact Object Mergers Powered by the Radioactive Decay of R-process Nuclei. Mon. Not. Roy. Astron. Soc. **406**, 2650 (2010). https://doi.org/10.1111/j.1365-2966.2010.16864.x
87. J. Barnes, D. Kasen, Effect of a High Opacity on the Light Curves of Radioactively Powered Transients from Compact Object Mergers. Astrophys. J. **775**, 18 (2013). arXiv:1303.5787. https://doi.org/10.1088/0004-637X/775/1/18
88. M. Tanaka, K. Hotokezaka, Radiative Transfer Simulations of Neutron Star Merger Ejecta. Astrophys. J. **775**, 113 (2013). arXiv:1306.3742. https://doi.org/10.1088/0004-637X/775/2/113
89. J. Barnes, D. Kasen, M.-R. Wu, G. Martínez-Pinedo, Radioactivity and thermalization in the ejecta of compact object mergers and their impact on kilonova light curves. Astrophys. J. **829**(2), 110 (2016). arXiv:1605.07218. https://doi.org/10.3847/0004-637X/829/2/110
90. R. T. Wollaeger, O. Korobkin, C. J. Fontes, S. K. Rosswog, W. P. Even, C. L. Fryer, J. Sollerman, A. L. Hungerford, D. R. van Rossum, A. B. Wollaber, Impact of ejecta morphology and composition on the electromagnetic signatures of neutron star mergers. Mon. Not. Roy. Astron. Soc. **478**(3), 3298–3334 (2018). arXiv:1705.07084. https://doi.org/10.1093/mnras/sty1018
91. M. Tanaka, *et al*, Kilonova from post-merger ejecta as an optical and near-infrared counterpart of GW170817. Publ. Astron. Soc. Jap. **69**(6), 12 (2017). arXiv:1710.05850. https://doi.org/10.1093/pasj/psx121
92. E. Waxman, E. O. Ofek, D. Kushnir, A. Gal-Yam, Constraints on the ejecta of the GW170817 neutron-star merger from its electromagnetic emission. Mon. Not. Roy. Astron. Soc. **481**(3), 3423–3441 (2018). arXiv:1711.09638. https://doi.org/10.1093/mnras/sty2441
93. M. W. Coughlin, *et al*, Constraints on the neutron star equation of state from AT2017gfo using radiative transfer simulations. Mon. Not. Roy. Astron. Soc. **480**(3), 3871–3878 (2018). arXiv:1805.09371. https://doi.org/10.1093/mnras/sty2174
94. K. Hotokezaka, E. Nakar, Radioactive heating rate of r-process elements and macronova light curve (2019). arXiv:1909.02581. https://doi.org/10.3847/1538-4357/ab6a98
95. K. Kawaguchi, M. Shibata, M. Tanaka, Diversity of Kilonova Light Curves. Astrophys. J. **889**(2), 171 (2020). arXiv:1908.05815. https://doi.org/10.3847/1538-4357/ab61f6
96. M. Ristic, E. Champion, R. O'Shaughnessy, R. Wollaeger, O. Korobkin, E. A. Chase, C. L. Fryer, A. L. Hungerford, C. J. Fontes, Interpolating detailed simulations of kilonovae: Adaptive learning and parameter inference applications. Phys. Rev. Res. **4**(1), 013046 (2022). arXiv:2105.07013. https://doi.org/10.1103/PhysRevResearch.4.013046
97. M. Breschi, A. Perego, S. Bernuzzi, W. Del Pozzo, V. Nedora, D. Radice, D. Vescovi, AT2017gfo: Bayesian inference and model selection of multicomponent kilonovae and constraints on the neutron star equation of state. Mon. Not. Roy. Astron. Soc. **505**(2), 1661–1677 (2021). arXiv:2101.01201. https://doi.org/10.1093/mnras/stab1287
98. S. Rosswog, U. Feindt, O. Korobkin, M.-R. Wu, J. Sollerman, A. Goobar, G. Martinez-Pinedo, Detectability of compact binary merger macronovae. Class. Quant. Grav. **34**(10), 104001 (2017). arXiv:1611.09822. https://doi.org/10.1088/1361-6382/aa68a9
99. S. Wanajo, Physical Conditions for the r-process. I. Radioactive Energy Sources of Kilonovae. Astrophys. J. **868**(1), 65 (2018). arXiv:1808.03763. https://doi.org/10.3847/1538-4357/aae0f2
100. J. Barnes, Y. L. Zhu, K. A. Lund, T. M. Sprouse, N. Vassh, G. C. McLaughlin, M. R. Mumpower, R. Surman, Kilonovae Across the Nuclear Physics Landscape: The Impact of Nuclear Physics Uncertainties on r-process-powered Emission. Astrophys. J. **918**(2), 44 (2021). arXiv:2010.11182. https://doi.org/10.3847/1538-4357/ac0aec
101. K. Hotokezaka, S. Wanajo, M. Tanaka, A. Bamba, Y. Terada, T. Piran, Radioactive decay products in neutron star merger ejecta: heating efficiency and γ-ray emission. Mon. Not. Roy. Astron. Soc. **459**(1), 35–43 (2016). arXiv:1511.05580. https://doi.org/10.1093/mnras/stw404
102. K. Hotokezaka, M. Tanaka, D. Kato, G. Gaigalas, Nebular emission from lanthanide-rich ejecta of neutron star merger. Mon. Not. Roy. Astron. Soc. **506**(4), 5863–5877 (2021). arXiv:2102.07879. https://doi.org/10.1093/mnras/stab1975
103. Q. Pognan, A. Jerkstrand, J. Grumer, On the validity of steady-state for nebular phase kilonovae. Mon. Not. Roy. Astron. Soc. **510**(3), 3806–3837 (2022). arXiv:2112.07484. https://doi.org/10.1093/mnras/stab3674
104. L.-X. Li, Radioactive Gamma-Ray Emissions from Neutron Star Mergers. Astrophys. J. **872**(1), 19 (2019). arXiv:1808.09833. https://doi.org/10.3847/1538-4357/aaf961
105. O. Korobkin, et al., Gamma-rays from kilonova: a potential probe of r-process nucleosynthesis (2019). arXiv:1905.05089. https://doi.org/10.3847/1538-4357/ab64d8
106. X. Wang, N. Vassh, T. Sprouse, M. Mumpower, R. Vogt, J. Randrup, R. Surman, MeV Gamma Rays from Fission: A Distinct Signature of Actinide Production in Neutron Star Mergers. Astrophys. J. Lett. **903**(1), 3 (2020). arXiv:2008.03335. https://doi.org/10.3847/2041-8213/abbe18
107. M.-H. Chen, L.-X. Li, D.-B. Lin, E.-W. Liang, Gamma-Ray Emission Produced by r-process Elements from Neutron Star Mergers. Astrophys. J. **919**(1), 59 (2021). arXiv:2107.02982. https://doi.org/10.3847/1538-4357/ac1267
108. M.-H. Chen, R.-C. Hu, E.-W. Liang, Radioactively-Powered Gamma-Ray Transient Associated with a Kilonova from Neutron Star Merger. Astrophys. J. Lett. **932**(1), L7 (2022). https://doi.org/10.3847/2041-8213/ac7470
109. M.-R. Wu, P. Banerjee, B. D. Metzger, G. Martínez-Pinedo, T. Aramaki, E. Burns, C. J. Hailey, J. Barnes, G. Karagiorgi, Finding the remnants of the Milky Way's last neutron star mergers. Astrophys. J. **880**(1), 23 (2019). arXiv:1905.03793. https://doi.org/10.3847/1538-4357/ab2593
110. Y. Terada, Y. Miwa, H. Ohsumi, S.-i. Fujimoto, S. Katsuda, A. Bamba, R. Yamazaki, Gamma-ray Diagnostics of r-process Nucleosynthesis in the Remnants of Galactic Binary Neutron-Star Mergers (2022). https://doi.org/10.48550/arXiv.2205.05407
111. T. Suda, Y. Katsuta, S. Yamada, T. Suwa, C. Ishizuka, Y. Komiya, K. Sorai, M. Aikawa, M. Y. Fujimoto, Stellar Abundances for the Galactic Archeology (SAGA) Database — Compilation of the Characteristics of Known Extremely Metal-Poor Stars. Publ. Astron. Soc. Japan. **60**, 1159 (2008). arXiv:0806.3697. https://doi.org/10.1093/pasj/60.5.1159

112. J. A. Johnson, M. Bolte, Th Ages for Metal-poor Stars. Astrophys. J. **554**(2), 888–902 (2001). arXiv:astro-ph/0103299. https://doi.org/10.1086/321386
113. J. J. Cowan, C. Sneden, S. Burles, I. I. Ivans, T. C. Beers, J. W. Truran, J. E. Lawler, F. Primas, G. M. Fuller, B. Pfeiffer, K.-L. Kratz, The Chemical Composition and Age of the Metal-poor Halo Star BD +17°3248. Astrophys. J. **572**(2), 861–879 (2002). arXiv:astro-ph/0202429. https://doi.org/10.1086/340347
114. V. Hill, B. Plez, R. Cayrel, T. C. Beers, B. Nordström, J. Andersen, M. Spite, F. Spite, B. Barbuy, P. Bonifacio, E. Depagne, P. François, F. Primas, First stars. I. The extreme r-element rich, iron-poor halo giant CS 31082-001. Implications for the r-process site(s) and radioactive cosmochronology. Astron. Astrophys. **387**, 560–579 (2002). arXiv:astro-ph/0203462. https://doi.org/10.1051/0004-6361:20020434
115. S. Honda, W. Aoki, T. Kajino, H. Ando, T. C. Beers, H. Izumiura, K. Sadakane, M. Takada-Hidai, Spectroscopic Studies of Extremely Metal-Poor Stars with the Subaru High Dispersion Spectrograph. II. The r-Process Elements, Including Thorium. Astrophys. J. **607**(1), 474–498 (2004). arXiv:astro-ph/0402298. https://doi.org/10.1086/383406
116. I. I. Ivans, J. Simmerer, C. Sneden, J. E. Lawler, J. J. Cowan, R. Gallino, S. Bisterzo, Near-Ultraviolet Observations of HD 221170: New Insights into the Nature of r-Process-rich Stars. Astrophys. J. **645**(1), 613–633 (2006). arXiv:astro-ph/0604180. https://doi.org/10.1086/504069
117. A. Frebel, N. Christlieb, J. E. Norris, C. Thom, T. C. Beers, J. Rhee, Discovery of HE 1523-0901, a Strongly r-Process-enhanced Metal-poor Star with Detected Uranium. Astrophys. J. Lett. **660**(2), 117–120 (2007). arXiv:astro-ph/0703414. https://doi.org/10.1086/518122
118. W. Aoki, S. Honda, K. Sadakane, N. Arimoto, First Determination of the Actinide Thorium Abundance for a Red Giant of the Ursa Minor Dwarf Galaxy. Publ. Astron. Soc. Japan. **59**, 15–19 (2007). arXiv:0704.3104. https://doi.org/10.1093/pasj/59.3.L15
119. D. K. Lai, M. Bolte, J. A. Johnson, S. Lucatello, A. Heger, S. E. Woosley, Detailed Abundances for 28 Metal-poor Stars: Stellar Relics in the Milky Way. Astrophys. J. **681**(2), 1524–1556 (2008). arXiv:0804.1370. https://doi.org/10.1086/588811
120. I. U. Roederer, K.-L. Kratz, A. Frebel, N. Christlieb, B. Pfeiffer, J. J. Cowan, C. Sneden, The End of Nucleosynthesis: Production of Lead and Thorium in the Early Galaxy. Astrophys. J. **698**(2), 1963–1980 (2009). arXiv:0904.3105. https://doi.org/10.1088/0004-637X/698/2/1963
121. I. U. Roederer, C. Sneden, I. B. Thompson, G. W. Preston, S. A. Shectman, Characterizing the Chemistry of the Milky Way Stellar Halo: Detailed Chemical Analysis of a Metal-poor Stellar Stream. Astrophys. J. **711**(2), 573–596 (2010). arXiv:1001.1745. [astro-ph.GA]. https://doi.org/10.1088/0004-637X/711/2/573
122. L. Mashonkina, N. Christlieb, P. S. Barklem, V. Hill, T. C. Beers, A. Velichko, The Hamburg/ESO R-process enhanced star survey (HERES). V. Detailed abundance analysis of the r-process enhanced star HE 2327-5642. Astron. Astrophys. **516**, 46 (2010). arXiv:1003.3571. https://doi.org/10.1051/0004-6361/200913825
123. I. U. Roederer, J. E. Lawler, J. S. Sobeck, T. C. Beers, J. J. Cowan, A. Frebel, I. I. Ivans, H. Schatz, C. Sneden, I. B. Thompson, New Hubble Space Telescope Observations of Heavy Elements in Four Metal-Poor Stars. Astrophys. J., Suppl. Ser. **203**(2), 27 (2012). arXiv:1210.6387. https://doi.org/10.1088/0067-0049/203/2/27
124. I. U. Roederer, G. W. Preston, I. B. Thompson, S. A. Shectman, C. Sneden, G. S. Burley, D. D. Kelson, A Search for Stars of Very Low Metal Abundance. VI. Detailed Abundances of 313 Metal-poor Stars. Astron. J. **147**(6), 136 (2014). arXiv:1403.6853. https://doi.org/10.1088/0004-6256/147/6/136
125. C. Siqueira Mello, V. Hill, B. Barbuy, M. Spite, F. Spite, T. C. Beers, E. Caffau, P. Bonifacio, R. Cayrel, P. François, H. Schatz, S. Wanajo, High-resolution abundance analysis of very metal-poor r-I stars. Astron. Astrophys. **565**, 93 (2014). arXiv:1404.0234. https://doi.org/10.1051/0004-6361/201423826
126. L. Mashonkina, N. Christlieb, K. Eriksson, The hamburg/eso r-process enhanced star survey (heres) - x. he 2252-4225, one more r-process enhanced and actinide-boost halo star. A&A. **569**, 43 (2014). https://doi.org/10.1051/0004-6361/201424017
127. V. M. Placco, E. M. Holmbeck, A. Frebel, T. C. Beers, R. A. Surman, A. P. Ji, R. Ezzeddine, S. D. Points, C. C. Kaleida, T. T. Hansen, C. M. Sakari, A. R. Casey, RAVE J203843.2-002333: The First Highly R-process-enhanced Star Identified in the RAVE Survey. Astrophys. J. **844**(1), 18 (2017). arXiv:1706.02934. https://doi.org/10.3847/1538-4357/aa78ef
128. E. M. Holmbeck, T. C. Beers, I. U. Roederer, V. M. Placco, T. T. Hansen, C. M. Sakari, C. Sneden, C. Liu, Y. S. Lee, J. J. Cowan, A. Frebel, The R-Process Alliance: 2MASS J09544277+5246414, the Most Actinide-enhanced R-II Star Known. Astrophys. J. Lett. **859**(2), 24 (2018). arXiv:1805.11925. https://doi.org/10.3847/2041-8213/aac722
129. C. M. Sakari, V. M. Placco, E. M. Farrell, I. U. Roederer, G. Wallerstein, T. C. Beers, R. Ezzeddine, A. Frebel, T. Hansen, E. M. Holmbeck, C. Sneden, J. J. Cowan, K. A. Venn, C. E. Davis, G. Matijevič, R. F. G. Wyse, J. Bland-Hawthorn, C. Chiappini, K. C. Freeman, B. K. Gibson, E. K. Grebel, A. Helmi, G. Kordopatis, A. Kunder, J. Navarro, W. Reid, G. Seabroke, M. Steinmetz, F. Watson, The R-Process Alliance: First Release from the Northern Search for r-process-enhanced Metal-poor Stars in the Galactic Halo. Astrophys. J. **868**(2), 110 (2018). arXiv:1809.09156. https://doi.org/10.3847/1538-4357/aae9df
130. I. U. Roederer, C. M. Sakari, V. M. Placco, T. C. Beers, R. Ezzeddine, A. Frebel, T. T. Hansen, The R-Process Alliance: A Comprehensive Abundance Analysis of HD 222925, a Metal-poor Star with an Extreme R-process Enhancement of [Eu/H] = -0.14. Astrophys. J. **865**(2), 129 (2018). arXiv:1808.09469. https://doi.org/10.3847/1538-4357/aadd92
131. M. Cain, A. Frebel, M. Gull, A. P. Ji, V. M. Placco, T. C. Beers, J. Meléndez, R. Ezzeddine, A. R. Casey, T. T. Hansen, I. U. Roederer, C. Sakari, The R-Process Alliance: Chemical Abundances for a Trio of r-process-enhanced Stars—One Strong, One Moderate, and One Mild. Astrophys. J. **864**(1), 43 (2018). arXiv:1807.03734. https://doi.org/10.3847/1538-4357/aad37d
132. M. Gull, A. Frebel, M. G. Cain, V. M. Placco, A. P. Ji, C. Abate, R. Ezzeddine, A. I. Karakas, T. T. Hansen, C. Sakari, E. M. Holmbeck, R. M. Santucci, A. R. Casey, T. C. Beers, The R-Process Alliance: Discovery of the First Metal-poor Star with a Combined r- and s-process Element Signature. Astrophys. J. **862**(2), 174 (2018). arXiv:1806.00645. https://doi.org/10.3847/1538-4357/aacbc3
133. C. M. Sakari, V. M. Placco, T. Hansen, E. M. Holmbeck, T. C. Beers, A. Frebel, I. U. Roederer, K. A. Venn, G. Wallerstein, C. E. Davis, E. M. Farrell, D. Yong, The r-process Pattern of a Bright, Highly r-process-enhanced Metal-poor Halo Star at [Fe/H] ∼ -2. Astrophys. J. Lett. **854**(2), 20 (2018). arXiv:1801.07727. https://doi.org/10.3847/2041-8213/aaa9b4
134. A. P. Ji, A. Frebel, From Actinides to Zinc: Using the Full Abundance Pattern of the Brightest Star in Reticulum II to Distinguish between Different r-process Sites. Astrophys. J. **856**(2), 138 (2018). arXiv:1802.07272. https://doi.org/10.3847/1538-4357/aab14a
135. T. C. Beers, N. Christlieb, The Discovery and Analysis of Very Metal-Poor Stars in the Galaxy. Annu. Rev. Astron. Astrophys. **43**(1), 531–580 (2005). https://doi.org/10.1146/annurev.astro.42.053102.134057
136. T. C. Beers, G. W. Preston, S. A. Shectman, A Search for Stars of Very Low Metal Abundance. II. Astron. J. **103**, 1987 (1992). https://doi.org/10.1086/116207
137. C. Sneden, J. J. Cowan, J. E. Lawler, I. I. Ivans, S. Burles, T. C. Beers, F. Primas, V. Hill, J. W. Truran, G. M. Fuller, B. Pfeiffer, K.-L. Kratz, The Extremely Metal-poor, Neutron Capture-rich Star CS 22892-052: A Comprehensive Abundance Analysis. Astrophys. J. **591**(2), 936–953 (2003). arXiv:astro-ph/0303542. https://doi.org/10.1086/375491
138. I. U. Roederer, J. E. Lawler, E. A. Den Hartog, V. M. Placco, R. Surman, T. C. Beers, R. Ezzeddine, A. Frebel, T. T. Hansen, K. Hattori, E. M. Holmbeck, C. M. Sakari, The R-Process Alliance: A Nearly Complete R-Process Abundance Template Derived from Ultraviolet Spectroscopy of the R-Process-Enhanced Metal-Poor Star HD 222925. Astropart. J. Suppl. Ser. **260**(2), 27 (2022). https://doi.org/10.3847/1538-4365/ac5cbc
139. R. Diehl, *et al*, Radioactive Al-26 and massive stars in the galaxy. Nature. **439**, 45–47 (2006). arXiv:astro-ph/0601015. https://doi.org/10.1038/nature04364
140. W. Wang, T. Siegert, Z. G. Dai, R. Diehl, J. Greiner, A. Heger, M. Krause, M. Lang, M. M. M. Pleintinger, X. L. Zhang, Gamma-Ray Emission of ^{60}Fe and ^{26}Al Radioactivity in Our Galaxy. Astrophys. J. **889**(2), 169 (2020). arXiv:1912.07874. https://doi.org/10.3847/1538-4357/ab6336
141. G. B. Hudson, B. M. Kennedy, F. A. Podosek, C. M. Hohenberg, The early solar system abundance of ^{244}Pu as inferred from the St. Severin chondrite,. Lunar Planet. Sci. Conf. Proc. **19**, 547–557 (1989)
142. K. Hotokezaka, T. Piran, M. Paul, Short-lived ^{244}Pu Points to Compact Binary Mergers as Sites for Heavy r-process Nucleosynthesis. Nature Phys. **11**, 1042 (2015). arXiv:1510.00711. https://doi.org/10.1038/nphys3574
143. S. Nishimura, K. Kotake, M.-a. Hashimoto, S. Yamada, N. Nishimura, S. Fujimoto, K. Sato, r-Process Nucleosynthesis in Magnetohydrodynamic

Jet Explosions of Core-Collapse Supernovae. Astrophys. J. **642**(1), 410–419 (2006). arXiv:astro-ph/0504100. https://doi.org/10.1086/500786

144. C. Winteler, R. Käppeli, A. Perego, A. Arcones, N. Vasset, N. Nishimura, M. Liebendörfer, F.-K. Thielemann, Magnetorotationally Driven Supernovae as the Origin of Early Galaxy *r*-process Elements? Astrophys. J. Lett. **750**, 22 (2012). arXiv:1203.0616. https://doi.org/10.1088/2041-8205/750/1/L22
145. P. Mösta, L. F. Roberts, G. Halevi, C. D. Ott, J. Lippuner, R. Haas, E. Schnetter, r-process Nucleosynthesis from Three-dimensional Magnetorotational Core-collapse Supernovae. Astrophys. J. **864**(2), 171 (2018). arXiv:1712.09370. https://doi.org/10.3847/1538-4357/aad6ec

Publisher's Note